RADIATIVE CORRECTIONS IN THE MSSM BEYOND ONE-LOOP: PRECISION OBSERVABLES AND NEUTRAL HIGGS MASSES

W. HOLLIK

Theoretical Physics Division, CERN, CH-1211 Geneva 23, Switzerland
and
Institut für Theoretische Physik, Universität Karlsruhe, D-76128 Karlsruhe, Germany
E-mail: Wolfgang.Hollik@physik.uni-karlsruhe.de

Recent results on two-loop QCD corrections to electroweak precision observables and to the neutral Higgs boson masses in the Minimal Supersymmetric Standard Model are presented. Main emphasis is on the QCD corrections to electroweak precision observables via squark contributions to the ρ-parameter, and on the Feynman-diagrammatic calculation of the masses of the MSSM Higgs bosons h^0, H^0 yielding the currently most precise prediction of the lightest Higgs mass m_h within the Feynman-graph approach.

1 Precision observables

Supersymmetry (SUSY)predicts the existence of scalar partners to each standard model (SM) fermion, and spin–1/2 partners to the gauge and Higgs bosons. So far, the direct search of SUSY particles at colliders has not been successful, and under some assumptions one can only set lower bounds on their masses [1].

An alternative way to probe SUSY is to search for the virtual effects of the additional particles. One can use the high-precison measurements of electroweak observables to search for the quantum effects of the SUSY particles. In the Minimal Supersymmetric Standard Model (MSSM) one finds two types of potentially large effects: The first possibility is that charginos and scalar top quarks are light enough to affect the decay width of the Z boson into b–quarks [2]; however, for masses beyond the LEP2 or Tevatron reach, these effects become too small to be observable [3].

The second possibility is the contribution of the top and bottom squark loops to the electroweak gauge–boson self–energies [4]: if there is a large splitting between the masses of these particles, the contribution will grow with the mass of the heaviest scalar quark and can be sizable. This is similar to the SM case, where the top/bottom weak isodoublet generates a quantum correction that grows as m_t^2. This contribution enters the electroweak observables via the ρ parameter [5], which influences the normalization of the NC Z couplings, the effective electroweak mixing angle at the Z–boson resonance and the $W-Z$ mass correlation.

The ρ parameter, in terms of the transverse parts of the W– and Z–boson self–energies at zero momentum–transfer, is given by

$$\rho = \frac{1}{1-\Delta\rho} \; ; \; \Delta\rho = \frac{\Pi_{ZZ}(0)}{M_Z^2} - \frac{\Pi_{WW}(0)}{M_W^2} \; . \qquad (1)$$

In the SM, the contribution of a fermion isodoublet (u,d) to $\Delta\rho$ reads at one–loop order

$$\Delta\rho_0^{\rm SM} = \frac{N_c G_F}{8\sqrt{2}\pi^2} F_0\left(m_u^2, m_d^2\right) \; , \qquad (2)$$

with the color factor N_c and the function F_0 given by

$$F_0(x,y) = x + y - \frac{2xy}{x-y}\log\frac{x}{y} \; . \qquad (3)$$

The only relevant SM contribution is due to the top/bottom weak isodoublet. Because $m_t \gg m_b$, one obtains $\Delta\rho_0^{\rm SM} = 3G_F m_t^2/(8\sqrt{2}\pi^2)$. The two-loop QCD corrections have been calculated long ago [6], yielding: $\Delta\rho_1^{\rm SM} = -\Delta\rho_0^{\rm SM}\cdot\frac{2}{3}\frac{\alpha_s}{\pi}(1+\pi^2/3)$. Meanwhile the three-loop term is also avialable [7]. The QCD corrections decrease the one–loop result by approximately 10%, corresponding to a shift of $\sim +10$ GeV in the indirect determination of the top mass.

In order to treat the SUSY loop contributions to the electroweak observables at the same level of accuracy as the standard contribution, higher order corrections should be incorporated. In particular the QCD corrections, which because of the large value of the strong coupling constant can be rather important, have to be included. They have been derived in ref [8], and will be briefly discussed here.

In SUSY theories, the scalar partners of each SM quark will induce additional contributions. The current eigenstates, $\tilde{q}_L$ and $\tilde{q}_R$, mix to give the mass eigenstates. The mixing angle is proportional to the quark mass and therefore is important only in the case of the third generation scalar quarks [9]. In particular, due to the large value of m_t, the mixing angle $\theta_{\tilde{t}}$ between $\tilde{t}_L$ and $\tilde{t}_R$ can be very large and lead to a scalar top quark $\tilde{t}_1$ much lighter than the t–quark and all the scalar partners of the light quarks [9]. The mixing in the $\tilde{b}$–quark sector can be sizable only in a small area of the SUSY parameter space.

Neglecting the mixing in the $\tilde{b}$ sector, $\Delta\rho$ is given at one–loop order by the simple expression

$$\Delta\rho_0^{\rm SUSY} = \frac{3G_F}{8\sqrt{2}\pi^2}\left[-\sin^2\theta_{\tilde{t}}\cos^2\theta_{\tilde{t}}F_0\left(m^2_{\tilde{t}_1},m^2_{\tilde{t}_2}\right)\right.$$
$$\left.+\cos^2\theta_{\tilde{t}}F_0\left(m^2_{\tilde{t}_1},m^2_{\tilde{b}_L}\right)+\sin^2\theta_{\tilde{t}}F_0\left(m^2_{\tilde{t}_2},m^2_{\tilde{b}_L}\right)\right]. \quad (4)$$

In a large area of the parameter space, the scalar top mixing angle is either very small $\theta_t \sim 0$ or maximal, $\theta_t \sim -\pi/4$. The contribution can be at the level of several per mille and is therefore within the range of the experimental observability. Relaxing the assumption of a common scalar quark mass, the corrections can become even larger [4,8].

At $\mathcal{O}(\alpha\alpha_s)$, the two–loop Feynman diagrams contributing to the ρ parameter in SUSY consist of two sets which are separately ultraviolet finite and gauge-invariant: diagrams involving only gluon exchange, and diagrams involving scalar quarks, gluinos, and quarks. The two–loop Feynman diagrams have to be supplemented by the corresponding one-loop counterterm insertions. The mass renormalization is performed in the on–shell scheme, where the mass is defined as the pole of the propagator. The mixing angle renormalization is performed in such a way that all transitions from $\tilde{q}_i \leftrightarrow \tilde{q}_j$ which do not depend on the loop–momenta in the two–loop diagrams are canceled.

The contribution of the $(\tilde{t},\tilde{b})$ doublet to the ρ parameter, including the two–loop gluon exchange and pure scalar quark diagrams in the case where the $\tilde{b}$ mixing is neglected, is given by an expression similar to Eq. (4):

$$\Delta\rho_1^{\rm SUSY} = \frac{G_F\alpha_s}{4\sqrt{2}\pi^3}\left[-\sin^2\theta_{\tilde{t}}\cos^2\theta_{\tilde{t}}F_1\left(m^2_{\tilde{t}_1},m^2_{\tilde{t}_2}\right)\right.$$
$$\left.+\cos^2\theta_{\tilde{t}}F_1\left(m^2_{\tilde{t}_1},m^2_{\tilde{b}_L}\right)+\sin^2\theta_{\tilde{t}}F_1\left(m^2_{\tilde{t}_2},m^2_{\tilde{b}_L}\right)\right]. \quad (5)$$

The two–loop function $F_1(x,y)$ is given in terms of dilogarithms by

$$F_1(x,y) = x+y-2\frac{xy}{x-y}\log\frac{x}{y}\left[2+\frac{x}{y}\log\frac{x}{y}\right]$$
$$+\frac{(x+y)x^2}{(x-y)^2}\log^2\frac{x}{y}-2(x-y){\rm Li}_2\left(1-\frac{x}{y}\right). \quad (6)$$

In the case of large mass splitting it increases with the heavy scalar quark mass squared: $F_1(x,0) = x(1+\pi^2/3)$.

The two–loop gluonic SUSY contribution to $\Delta\rho$ is shown in Fig. 1 as a function of the common scalar mass $m_{\tilde{q}}$, for the two scenarios discussed previously: $\theta_{\tilde{t}} = 0$ and $\theta_{\tilde{t}} \simeq -\pi/4$. The two–loop contribution is of the order of 10 to 15% of the one–loop result. Contrary to the SM case where the two–loop correction screens the one–loop contribution, $\Delta\rho_1^{\rm SUSY}$ has the same sign as $\Delta\rho_0^{\rm SUSY}$. In

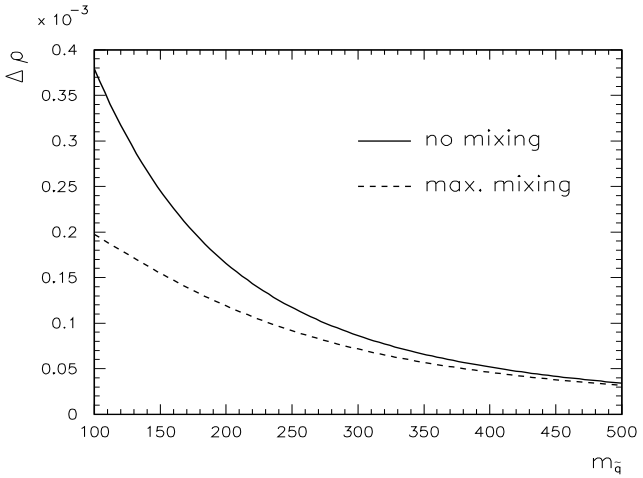

Figure 1: Gluon exchange contribution to the ρ parameter at two–loop as a function of the common mass $m_{\tilde{q}}$, for $\theta_{\tilde{t}} = 0$ and $\theta_{\tilde{t}} \sim -\pi/4$ [with $\tan\beta = 1.6$ and $M_t^{\rm LR} = 0$ and 200 GeV, respectively, where $M_t^{\rm LR}$ is the off–diagonal term in the $\tilde{t}$ mass matrix].

the case of degenerate $\tilde{t}$ squarks with masses $m_{\tilde{t}} \gg m_{\tilde{b}}$, the result is the same as the QCD correction to the (t,b) contribution in the SM, but with opposite sign. The gluonic correction to the contribution of scalar quarks to the ρ parameter will therefore enhance the sensitivity in the search of the virtual effects of scalar quarks in high–precision electroweak measurements.

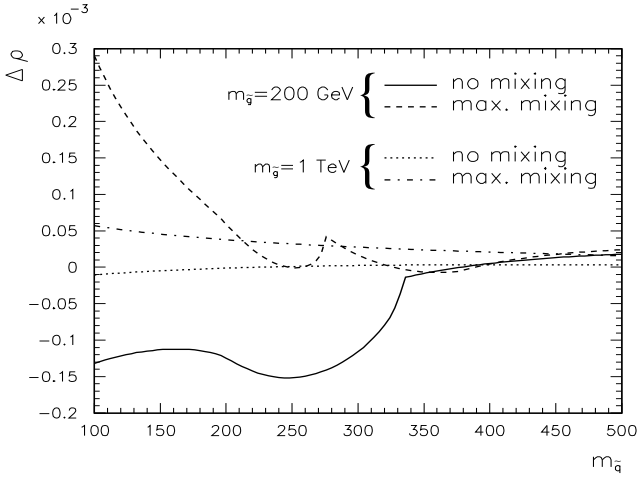

Figure 2: Contribution of the gluino exchange diagrams to $\Delta\rho_1^{\rm SUSY}$ for two values of $m_{\tilde{g}}$ in the scenarios of Fig. 1.

The gluino exchange diagrams cannot be cast into a simple anlytical expression. In general they give smaller contributions compared to gluon exchange. Only for gluino and scalar quark masses close to the experimental lower bounds they compete with the gluon exchange contributions. In this case, the gluon and gluino contributions add up to $\sim$ 30% of the one–loop value for maximal mixing [Fig. 2]. For larger values of $m_{\tilde{g}}$, the

contribution decreases rapidly since the gluinos decouple for high masses.

2 Masses of the neutral Higgs bosons

The search for the lightest Higgs boson provides a direct and very stringent test of SUSY. A precise prediction for the mass of the lightest Higgs boson in terms of the relevant SUSY parameters hence is crucial in order to determine the discovery and exclusion potential of LEP2 and the upgraded Tevatron and also for physics at the LHC, where a high-precision measurement of the mass of this particle might be possible.

In the MSSM the mass of the lightest Higgs boson, m_h, is restricted at the tree level to be smaller than the Z-boson mass. This bound, however, is strongly affected by the inclusion of radiative corrections. The dominant one-loop corrections arise form the top and scalar-top sector via terms of the form $G_F m_t^4 \ln(m_{\tilde{t}_1} m_{\tilde{t}_2}/m_t^2)$ [10]. They increase the predicted values of m_h and yield an upper bound of about 150 GeV. These results have been improved by performing a complete one-loop calculation in the on-shell scheme, which takes into account the contributions of all sectors of the MSSM [11,12,13]. Beyond one-loop order renormalization group (RG) methods have been applied in order to obtain leading logarithmic higher-order contributions [14,15,16,17], and a diagrammatic calculation of the dominant two-loop contributions in the limiting case of vanishing $\tilde{t}$-mixing and infinitely large M_A and $\tan\beta$ has been carried out [18].

Recently a Feynman-diagrammatic calculation of the leading two-loop corrections of $\mathcal{O}(\alpha\alpha_s)$ to the masses of the neutral $\mathcal{CP}$-even Higgs bosons has been performed [19]. They have been combined with the complete one-loop diagrammatic calculation [20] to obtain in this way the currently most precise prediction for m_h within the Feynman-diagrammatic approach for arbitrary values of the parameters of the Higgs and scalar top sector of the MSSM. Further refinements concerning the leading two-loop Yukawa corrections of $\mathcal{O}(G_F^2 m_t^6)$ [15,21] and of leading QCD corrections beyond two-loop order are also included. The results will be discussed in this section.

In the MSSM two Higgs doublets are needed, decomposed as follows:

$$H_1 = \begin{pmatrix} H_1^1 \\ H_1^2 \end{pmatrix} = \begin{pmatrix} v_1 + (\phi_1^0 + i\chi_1^0)/\sqrt{2} \\ \phi_1^- \end{pmatrix},$$
$$H_2 = \begin{pmatrix} H_2^1 \\ H_2^2 \end{pmatrix} = \begin{pmatrix} \phi_2^+ \\ v_2 + (\phi_2^0 + i\chi_2^0)/\sqrt{2} \end{pmatrix}. \qquad (7)$$

The Higgs sector can be described with the help of two independent parameters (besides the gauge couplings g, g'), usually chosen as $\tan\beta = v_2/v_1$ and the mass M_A of the $\mathcal{CP}$-odd A boson. The $\mathcal{CP}$-even neutral mass eigenstates h^0, H^0 are obtained from $\phi_{1,2}^0$ by a rotation yielding the tree-level masses $m_{h,H,\mathrm{tree}}$.

In the Feynman-diagrammatic approach the one-loop corrected Higgs masses are derived by finding the poles of the $h - H$-propagator matrix whose inverse is given by

$$\begin{pmatrix} q^2 - m_{H,\mathrm{tree}}^2 + \hat{\Sigma}_H(q^2) & \hat{\Sigma}_{hH}(q^2) \\ \hat{\Sigma}_{hH}(q^2) & q^2 - m_{h,\mathrm{tree}}^2 + \hat{\Sigma}_h(q^2) \end{pmatrix}, \quad (8)$$

where the $\hat{\Sigma}$ denote the full one-loop contributions to the renormalized Higgs-boson self-energies. For these self-energies we take the result of the complete one-loop on-shell calculation of [12]. The agreement with the result obtained in [11] is better than 1 GeV for almost the whole MSSM parameter space.

As mentioned above the dominant contribution arises from the $t - \tilde{t}$-sector. The current eigenstates of the scalar quarks, $\tilde{q}_L$ and $\tilde{q}_R$, mix to give the mass eigenstates $\tilde{q}_1$ and $\tilde{q}_2$. The non-diagonal entry in the scalar quark mass matrix is proportional to the mass of the quark and reads for the $\tilde{t}$-mass matrix

$$m_t M_t^{LR} = m_t(A_t - \mu \cot\beta\,), \qquad (9)$$

where we have adopted the conventions used in [8]. Due to the large value of m_t mixing effects have to be taken into account. Diagonalizing the $\tilde{t}$-mass matrix one obtains the eigenvalues $m_{\tilde{t}_1}$ and $m_{\tilde{t}_2}$ and the $\tilde{t}$ mixing angle $\theta_{\tilde{t}}$.

The leading two-loop corrections have been obtained in [19] by calculating the $\mathcal{O}(\alpha\alpha_s)$ contribution of the $t - \tilde{t}$-sector to the renormalized Higgs-boson self-energies at zero external momentum from the Yukawa part of the theory. At the two-loop level the matrix (8) consists of the renormalized Higgs-boson self-energies

$$\hat{\Sigma}_s(q^2) = \hat{\Sigma}_s^{(1)}(q^2) + \hat{\Sigma}_s^{(2)}(0), \quad s = h, H, hH, \qquad (10)$$

where the momentum dependence is neglected only in the two-loop contribution. The Higgs-boson masses at the two-loop level are obtained by determining the poles of the matrix Δ_{Higgs} in Eq. (8).

We have implemented two further steps of refinement into the prediction for m_h, which are shown separately in the plots below. The leading two-loop Yukawa correction of $\mathcal{O}(G_F^2 m_t^6)$ is taken over from the result obtained by renormalization group methods [15,21]. The second step of refinement concerns leading QCD corrections beyond two-loop order, taken into account by using the $\overline{MS}$ top mass, $\overline{m}_t = \overline{m}_t(m_t) \approx 166.5$ GeV, for the two-loop contributions instead of the pole mass, $m_t = 175$ GeV. In the $\tilde{t}$ mass matrix, however, we continue to use the pole mass as an input parameter. Only when performing the comparison with the RG results we use $\overline{m}_t$ in the $\tilde{t}$ mass

matrix for the two-loop result, since in the RG results the running masses appear everywhere. This three-loop effect gives rise to a shift up to 1.5 GeV in the prediction for m_h.

For the numerical evaluation we have chosen two values for $\tan\beta$ which are favored by SUSY-GUT scenarios [22]: $\tan\beta = 1.6$ for the $SU(5)$ scenario and $\tan\beta = 40$ for the $SO(10)$ scenario. Other parameters are $M_Z = 91.187$ GeV, $M_W = 80.375$ GeV, $G_F = 1.16639\,10^{-5}$ GeV^{-2}, $\alpha_s(m_t) = 0.1095$, and $m_t = 175$ GeV. For the figures below we have furthermore chosen $M = 400$ GeV (M is the soft SUSY breaking parameter in the chargino and neutralino sector), $M_A = 500$ GeV, and $m_{\tilde{g}} = 500$ GeV as typical values (if not indicated differently). The scalar top masses and the mixing angle are derived from the parameters $M_{\tilde{t}_L}$, $M_{\tilde{t}_R}$ and M_t^{LR} of the $\tilde{t}$ mass matrix (our conventions are the same as in [8]). In the figures below we have chosen $m_{\tilde{q}} \equiv M_{\tilde{t}_L} = M_{\tilde{t}_R}$.

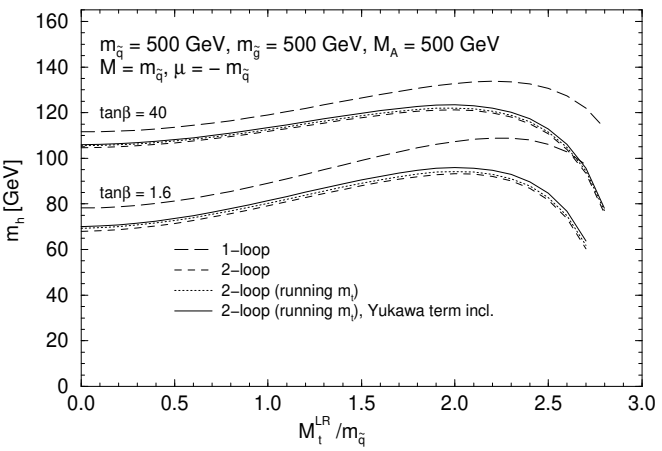

Figure 3: One- and two-loop results for m_h as a function of $M_t^{LR}/m_{\tilde{q}}$ for two values of $\tan\beta$.

The plot in Fig. 3 shows the result for m_h obtained from the diagrammatic calculation of the full one-loop and leading two-loop contributions. The two steps of refinement discussed above are shown in separate curves. For comparison the pure one-loop result is also given. The results are plotted as a function of $M_t^{LR}/m_{\tilde{q}}$, where $m_{\tilde{q}}$ is fixed to 500 GeV. The qualitative behavior is the same as in [19], where the result containing only the leading one-loop contribution (and without further refinements) was shown. The two-loop contributions give rise to a large reduction of the one-loop result of 10–20 GeV. The two steps of refinement both increase m_h by up to 2 GeV. A minimum occurs for $M_t^{LR} = 0$ GeV which we refer to as 'no mixing' (different from section 1). A maximum in the two-loop result for m_h is reached for about $M_t^{LR}/m_{\tilde{q}} \approx 2$ in the $\tan\beta = 1.6$ scenario as well as in the $\tan\beta = 40$ scenario. This case we refer to as 'maximal mixing' (differently from section 1). The maximum is shifted compared to its one-loop value of about $M_t^{LR}/m_{\tilde{q}} \approx 2.4$. The two steps of refinement have only a negligible effect on the location of the maximum.

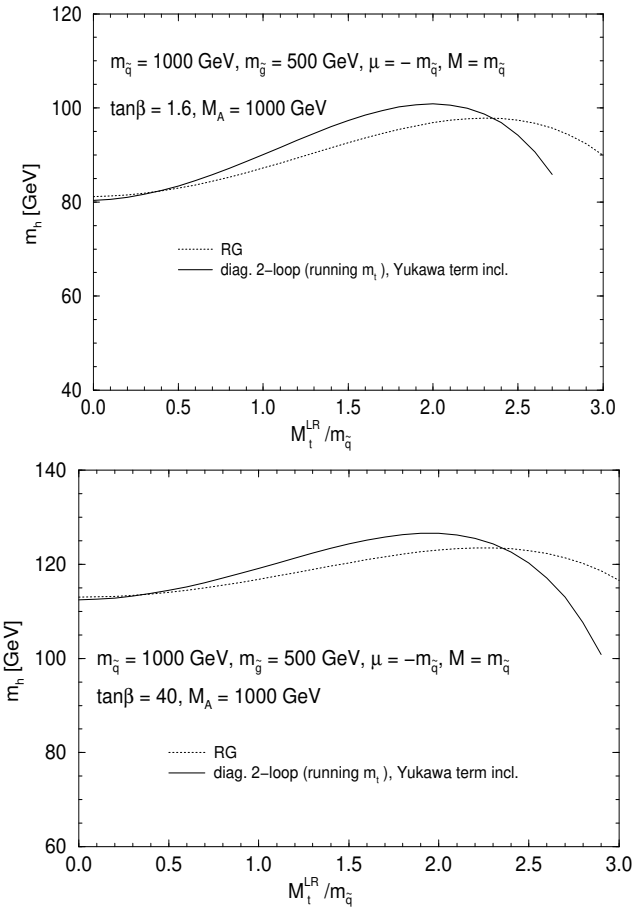

Figure 4: Comparison between the Feynman-diagrammatic calculations and the results obtained by renormalization group methods [16]. The mass of the lightest Higgs boson is shown for the two scenarios with $\tan\beta = 1.6$ and $\tan\beta = 40$ for increasing mixing in the $\tilde{t}$-sector and $m_{\tilde{q}} = M_A$.

We now turn to the comparison of our diagrammatic results with the predictions obtained via renormalization group methods. We begin with the case of vanishing mixing in the $\tilde{t}$ sector and large values of M_A, for which the RG approach is most easily applicable and is expected to work most accurately. In order to study different contributions separately, we have first compared the diagrammatic one-loop on-shell result [12] with the one-loop leading log result (without renormalization group improvement) given in [17] and found very good agreement, typically within 1 GeV. We then performed a leading log expansion of our diagrammatic result (which corresponds to the two-loop contribution in the RG approach) and

also found agreement with the full two-loop result within about 1 GeV. Finally, we have compared our diagrammatic result for the no-mixing case including the refinement terms with the RG results [a] obtained in [16]. After the inclusion of the refinement terms the diagrammatic result for the no-mixing case agrees very well with the RG result. The deviation between the results exceeds 2 GeV only for $\tan\beta = 1.6$ and $m_{\tilde{q}} < 150$ GeV. For smaller values of M_A the comparison for the no-mixing case looks qualitatively the same. For $\tan\beta = 1.6$ and values of M_A below 100 GeV slightly larger deviations are possible. Since the RG results do not contain the gluino mass as a parameter, varying $m_{\tilde{g}}$ gives rise to an extra deviation, which in the no-mixing case does not exceed 1 GeV. Varying the other parameters μ and M in general does not lead to a sizable effect in the comparison with the corresponding RG results.

We now consider the situation when mixing in the $\tilde{t}$ sector is taken into account. We have again compared the full one-loop result with the one-loop leading log result used within the RG approach [17] and found good agreement. Only for values of M_A below 100 GeV and large mixing deviations of about 5 GeV occur. In Fig. 4 our diagrammatic result including the refinement terms is compared with the RG results [16] as a function of $M_t^{LR}/m_{\tilde{q}}$ for $\tan\beta = 1.6$ and $\tan\beta = 40$. For larger $\tilde{t}$-mixing sizable deviations between the diagrammatic and the RG results occur, which can exceed 5 GeV for moderate mixing and become very large for large values of $M_t^{LR}/m_{\tilde{q}}$. As already stressed above, the maximal value for m_h in the diagrammatic approach is reached for $M_t^{LR}/m_{\tilde{q}} \approx 2$, whereas the RG results have a maximum at $M_t^{LR}/m_{\tilde{q}} \approx 2.4$, i.e. at the one-loop value. Varying the value of $m_{\tilde{g}}$ in our result leads to a larger effect than in the no-mixing case and shifts the diagrammatic result relative to the RG result within ± 2 GeV.

So far, the results of our diagrammatic on-shell calculation and the RG methods have been compared in terms of the parameters $M_{\tilde{t}_L}$, $M_{\tilde{t}_R}$ and M_t^{LR} of the $\tilde{t}$ mixing matrix, since the available numerical codes for the RG results [16,17] are given in terms of these parameters. However, since the two approaches rely on different renormalization schemes, the meaning of these (non-observable) parameters is not precisely the same in the two approaches starting from two-loop order. Indeed we have checked that assuming fixed values for the physical parameters $m_{\tilde{t}_1}$, $m_{\tilde{t}_2}$, and $\theta_{\tilde{t}}$ and deriving the corresponding values of the parameters $M_{\tilde{t}_L}$, $M_{\tilde{t}_R}$ and M_t^{LR} in the on-shell scheme as well as in the $\overline{MS}$ scheme, sizable differences occur between the values of the mixing parameter M_t^{LR} in the two schemes, while the parameters $M_{\tilde{t}_L}$, $M_{\tilde{t}_R}$ are approximately equal in the two schemes. Thus, part of the different shape of the curves in Fig. 4 may be attributed to a different meaning of the parameter M_t^{LR} in the on-shell scheme and in the RG calculation.

[a] The RG results of [16] and [17] agree within about 2 GeV with each other.

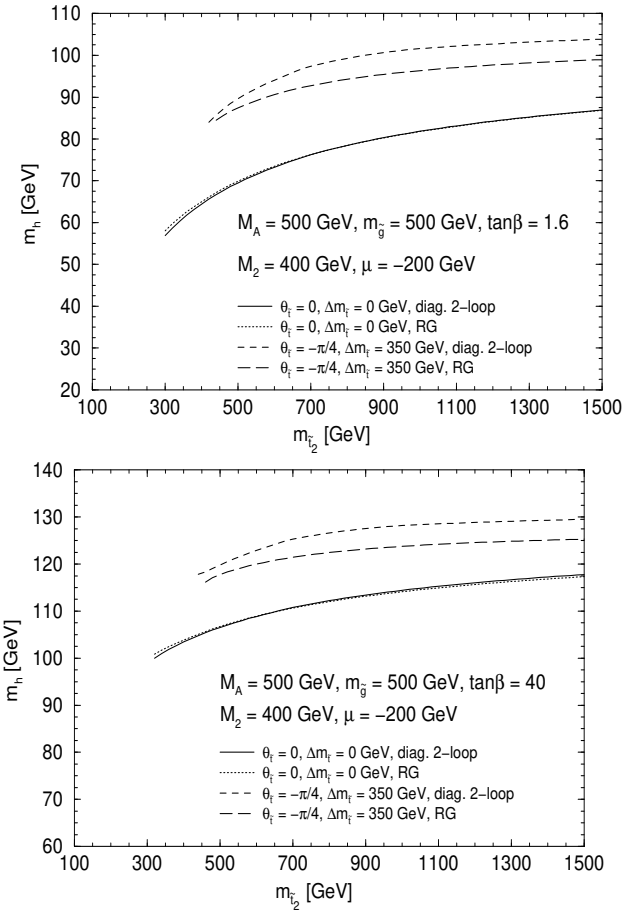

Figure 5: Comparison between the Feynman-diagrammatic calculations and the results obtained by renormalization group methods [16]. The mass of the lightest Higgs boson is shown for the two scenarios with $\tan\beta = 1.6$ and $\tan\beta = 40$ as a function of the heavier physical $\tilde{t}$ mass $m_{\tilde{t}_2}$. For the curves with $\theta_{\tilde{t}} = 0$ a mass difference $\Delta m_{\tilde{t}} = 0$ GeV is assumed whereas for $\theta_{\tilde{t}} = -\pi/4$ we chose $\Delta m_{\tilde{t}} = 350$ GeV, for which the maximal Higgs masses are achieved.

For the purpose of comparing results obtained in different renormalization schemes it is very desirable to express the prediction for the Higgs-boson masses in terms of physical observables, i.e. the physical masses and mixing angles of the model instead of unphysical parameters. As a step into this direction we compare in Fig. 5 the diagrammatic results and the RG results as a function of the physical mass $m_{\tilde{t}_2}$ and with the mass difference $\Delta m_{\tilde{t}} = m_{\tilde{t}_2} - m_{\tilde{t}_1}$ and the mixing angle $\theta_{\tilde{t}}$ as parameters. In the context of the RG approach the running $\tilde{t}$ masses, derived from the $\tilde{t}$ mass matrix, are considered as an approximation for the physical masses. The range of

the $\tilde{t}$ masses appearing in Fig. 5 has been constrained by requiring that the contribution of the third generation of scalar quarks to the ρ-parameter [8] does not exceed the value of $1.3 \cdot 10^{-3}$. As in the comparison performed above, in Fig. 5 very good agreement is found between the results of the two approaches in the case of vanishing $\tilde{t}$ mixing. For the maximal mixing angle $\theta_{\tilde{t}} = -\pi/4$, however, the diagrammatic result yields values for m_h which are higher by about 5 GeV.

References

1. D. Treille, plenary talk at ICHEP98, these proceedings
2. A. Djouadi, G. Girardi, W. Hollik, F. Renard, C. Verzegnassi, *Nucl. Phys.* B **349**, 48 (1991); M. Boulware, D. Finnell, *Phys. Rev.* D **44**, 2054 (1991)
3. W. de Boer et al., *Z. Phys.* C **75**, 627 (1997)
4. R. Barbieri et al., *Nucl. Phys.* B **224**, 32 (1983); M. Drees, K. Hagiwara, *Phys. Rev.* D **42**, 1709 (1990); P. Chankowski et al., *Nucl. Phys.* B **417**, 101 (1994)
5. M. Veltman, *Nucl. Phys.* B **123**, 89 (1977)
6. A. Djouadi, C. Verzegnassi, *Phys. Lett.* B **195**, 265 (1987); A. Djouadi, *Nuovo Cim.* A **100**, 357 (1988)
7. K. Chetyrkin, J. Kühn, M. Steinhauser, *Phys. Lett.* B **351**, 331 (1995); L. Avdeev et al., *Phys. Lett.* B **336**, 560 (1994), E: B **349**, 597 (1995)
8. A. Djouadi, P. Gambino. S. Heinemeyer, W. Hollik, C. Jünger, G. Weiglein, *Phys. Rev. Lett.* **78**, 3626 (1997); *Phys. Rev.* D **57**, 4179 (1998)
9. J. Ellis, S. Rudaz, *Phys. Lett.* B **128**, 248 (1983)
10. H. Haber, R. Hempfling, *Phys. Rev. Lett.* **66**, 1815 (1991); Y. Okada, M. Yamaguchi, T. Yanagida, *Prog. Theor. Phys.* **85**, 1 (1991); J. Ellis, G. Ridolfi, F. Zwirner, *Phys. Lett.* B **257**, 83 (1991); *Phys. Lett.* B **262**, 477 (1991); R. Barbieri, M. Frigeni, *Phys. Lett.* B **258**, 395 (1991)
11. P. Chankowski, S. Pokorski, J. Rosiek, *Nucl. Phys.* B **423**, 437 (1994)
12. A. Dabelstein, *Nucl. Phys.* B **456**, 25 (1995); *Z. Phys.* C **67**, 495 (1995)
13. J. Bagger, K. Matchev, D. Pierce, R. Zhang, *Nucl. Phys.* B **491**, 3 (1997)
14. J. Casas, J. Espinosa, M. Quirós, A. Riotto, *Nucl. Phys.* B **436**, 3 (1995), E: *ibid.* B **439**, 466 (1995)
15. M. Carena, J. Espinosa, M. Quirós, C. Wagner, *Phys. Lett.* B **355**, 209 (1995)
16. M. Carena, M. Quirós, C. Wagner, *Nucl. Phys.* B **461**, 407 (1996)
17. H. Haber, R. Hempfling, A. Hoang, *Z. Phys.* C **75**, 539 (1997)
18. R. Hempfling, A. Hoang, *Phys. Lett.* B **331**, 99 (1994)
19. S. Heinemeyer, W. Hollik, G. Weiglein, *Phys. Rev.* D **58**, 091701 (1998)
20. S. Heinemeyer, W. Hollik, G. Weiglein, hep-ph/9807423 (*Phys. Lett.* B , to appear)
21. M. Carena, P. Chankowski, S. Pokorski, C. Wagner, FERMILAB-PUB-98/146-T, hep-ph/9805349.
22. M. Carena, S. Pokorski, C. Wagner, *Nucl. Phys.* B **406**, 59 (1993); W. de Boer et al., *Z. Phys.* C **71**, 415 (1996)